Article

Inductive Compensation of an Open-Loop IPT Circuit: Analysis and Design

Mario Ponce-Silva *[ID], **Alan R. García-García** [ID], **Jaime Arau** [ID], **Josué Lara-Reyes** [ID] and **Claudia Cortés-García** [ID]

Tecnológico Nacional de México—CENIDET, Cuernavaca 62490, Mexico; alan.garcia18ee@cenidet.edu.mx (A.R.G.-G.)
* Correspondence: mario.ps@cenidet.tecnm.mx

Abstract: The main contribution of this paper is the inductive compensation of a wireless inductive power transmission circuit (IPT) with resonant open-loop inductive coupling. The variations in the coupling coefficient k due to the misalignment of the transmitter and receiver are compensated with only one auxiliary inductance in the primary of the inductive coupling. A low-power prototype was implemented with the following specifications: input voltage Vin = 27.5 V, output power Po = 10 W, switching frequency f = 500 kHz, output voltage Vo = 12 V, transmission distance d = 1.5 mm. Experimental results varying the distance "d" with several values of the compensation inductor demonstrate the feasibility of the proposal. An efficiency of 75.10% under nominal conditions was achieved. This proposal is a simple compensation topology for wireless chargers of cellular phones presenting small distances between the transmitter and receiver.

Keywords: cellular phones; inductive power transfer; resonant converter; DC-DC converter

1. Introduction

Nowadays, wireless power transmission (WPT) has become a trending research topic due to many applications involving no wired connections such as charging of electric vehicles, cell phones, hand tools, biomedical implants and portable electronics [1,2].

WPT has been used mainly in two applications—in the sending of information and electrical energy, or only for transmitting electrical energy. The second case shall be addressed in this work, with the aim of transmitting electrical power from a power supply to an electrical load, using a resonant inductive coupling [3–5].

WPT can be classified into two categories—far-field and near-field WPT. The far-field category refers to the transmission of a large amount of energy between two positions, e.g., sending energy by electromagnetic waves. Near-field WPT refers to the distance of transfer energy within the wavelength (λ) of the transmitter antenna [6–8]. This paper will focus on near-field WPT.

As shown in Figure 1, inductive power transmission (IPT) circuits consist of multiple stages of energy conversion to achieve the desired operation, usually as follows: low-frequency rectifier, high-frequency (HF) inverter with a resonant tank, inductive coupling with a coupling factor k, high-frequency rectifier, and load [9–11]. This work is focused on the stages from the HF inverter only.
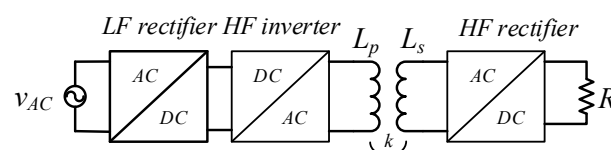

Figure 1. Typical structure of inductive power transmission (IPT) circuit.

An indispensable stage in IPT circuits is the resonant tank, also known as resonant network, which is an electrical circuit designed with capacitors and inductors which is capable of storing electrical energy and oscillating when it is operating at the resonant frequency. The circuit has zero reactance during the resonance condition, allowing the maximum transfer of power from a power supply to an electrical load with high efficiency [12,13].

In low-power resonant IPT applications, such as wireless chargers for smartphones and portable electronic devices (less than 20 W), the literature reports efficiencies of approximately 50–70% in open-loop operation and 70–80% in closed-loop operation [14,15].

Usually, the IPT topologies require compensation networks to operate the circuit in resonance. The basic compensation networks are presented in Figure 2; as can be seen, the compensation networks include a capacitor in series or parallel with the transmitter and the receiver to compensate for their inductance and to operate at resonance [16,17].
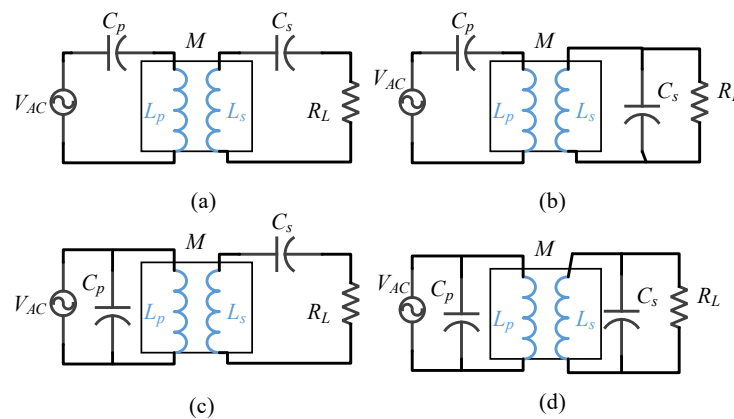

Figure 2. Basic compensation networks. (**a**) series-series, (**b**) series-parallel, (**c**) parallel-series, (**d**) parallel-parallel.

The full circuit needs many components to achieve optimal operation; these components cause additional losses, thus diminishing the efficiency. One solution is to consider the parasitic components (leakage inductances) and use them as part of the design to achieve high efficiency, fewer components, and better power transfer in inductive coupling [18,19].

Many compensation topologies have been proposed to compensate for the leakage inductances. The most used compensation topologies consist of adding one capacitor in series with each leakage inductance C_p and C_s (Figure 3). Both capacitors are chosen to be in resonance with each leakage inductance [20–22].
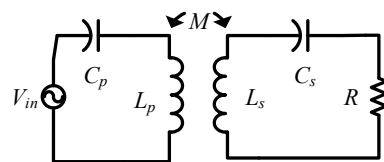

Figure 3. Resonance conditions used in the literature for IPT circuits.

Table 1 shows some reported circuits with their most important operating characteristics. This table shows that a higher operating power results in better overall efficiency of the circuit. In addition, Table 1 allows comparing the results obtained in this paper with those reported in the literature, where even though in this paper a low power of 10 W was used, an efficiency of up to 75% was achieved, which is higher than some of the circuits shown in Table 1 with similar power levels.

The main contribution of this paper is to eliminate the compensation capacitor C_s in the receiver, compensate for the misalignment of the transmitter and the receiver with only

one series capacitor in the transmitter, and add an inductor in series with this capacitor to compensate for the changes in the mutual inductance M.

Table 1. Comparison of reported resonant circuits with applications in wireless power transmission.

Frequency	Output Power	Coupling Factor	Efficiency	Ref.
140 kHz	80 W	0.24	60.70%	[23]
40 kHz	45 W	0.25	70.60%	[24]
82.3 kHz	10 W	0.059	50%	[25]
1 MHz	100 W	0.25	92%	[26]
800 kHz	12 W	0.1	56%	[27]
450 kHz	300 W	0.32	75%	[28]
500 kHz	2 W	0.05	65%	[29]
120 kHz	10 W	0.3	69%	[30]

The proposal simplifies the secondary circuit and reduces the complexity of the circuit, with a higher efficiency than the works reported in Table 1. This contribution is particularly relevant in low-power applications where low size and cost are important, such as biomedical implants, portable electronics, electro mobility, and Internet of Things applications.

2. Analysis of the Circuit

The IPT circuits are usually modelled as two coupled inductors as shown in Figure 4a, with a coupling factor k defined as:

$$k = \frac{M}{\sqrt{L_1 L_2}} \tag{1}$$

where M is the mutual inductance, L_1 is the self-inductance of the primary (transmitter) and L_2 is the self-inductance of the secondary (receiver). This model is commonly employed and useful in the literature.
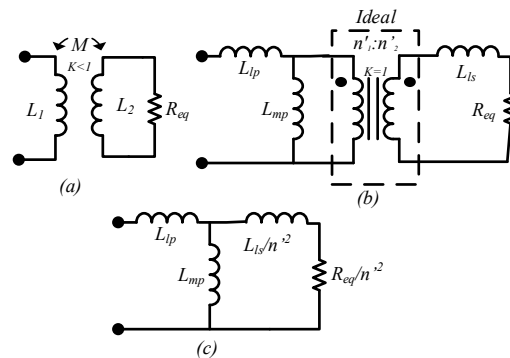

Figure 4. Models of IPT circuits. (**a**) Typical model using coupling inductors. (**b**) Model T of the coupled inductors using an ideal transformer, (**c**) model T with secondary reflected to the primary.

The main disadvantage is that the model separates the analysis of the circuit into two parts—primary and secondary. To merge both circuits in only one, model T is the usual selection [31,32].

Model T could be rearranged as the circuit in Figure 4b. This circuit models the mutual inductance M as an ideal transformer with coupling factor $k = 1$ and turn relationship $n' = n'_2/n'_1$; turns n'_1 and n'_2 represent the cross section of coils L_1 and L_2 that share the same common flux φ_M and are different from the total turn number of each inductor L_1 (n_1) and L_2 (n_2). The components of this model are related to the model in Figure 3b as shown in Table 2.

Figure 4c shows the elements of the secondary reflected to the primary of the ideal transformer; this last model was the model used in this analysis. The proposed circuit to

be analyzed in this paper is presented in Figure 5. The HF inverter consists of a half bridge inverter with a compensation topology that is only made up of the compensation inductor L_C and the capacitor C_p. The IPT transformer is modelled like the model in Figure 4b, where the HF AC–DC conversion consists of a conventional full bridge rectifier.

Table 2. Relationships among the coupling inductances models.

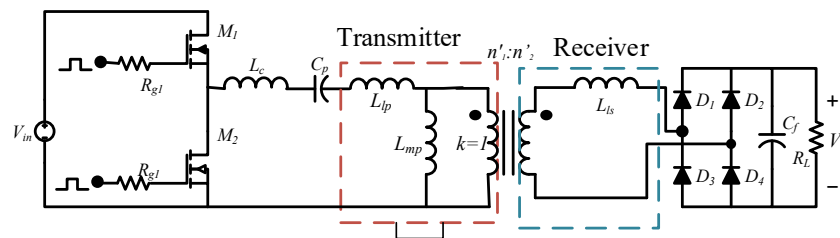| Parameter	Description	Value
L_{lp}	Primary leakage inductance	$L_{lp} = L_1 - M$
L_{ls}	Secondary leakage inductance	$L_{ls} = L_2 - M$
L_{mp}	Primary magnetizing inductance	$L_{mp} = \frac{n'_1}{n'_2} M = \frac{M}{n'}$

Figure 5. IPT circuit analyzed.

To compensate for the variations due to the misalignment of the transmitter and receiver, as well as variations caused by the increase in the distance between the transmitter and receiver, the compensation inductor L_c will have a value greater than 90% of the inductive reactance at resonant conditions. The remaining percentage of the inductive reactance belongs to the primary dispersion inductance L_{lp} and the equivalent inductance L_{eq1} obtained from the inductive coupling.

To analyze the resonant network, the resonant converter shown in Figure 5 is simplified until an equivalent circuit is obtained in series, in which the resonance condition will be established. Figure 6 shows the simplification process.
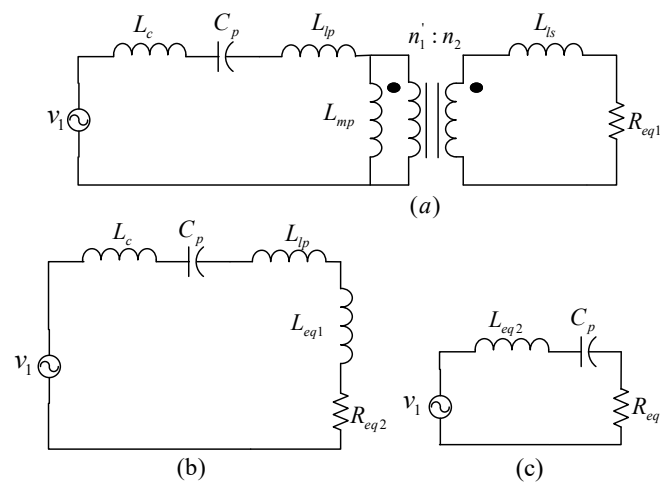
Figure 6. Analysis of the IPT circuit to obtain the resonance condition, (**a**) simplified IPT circuit with the equivalent resistance of the rectifier, (**b**) circuit obtained by reflecting the circuit secondary to the primary circuit, (**c**) total series equivalent circuit where the resonance condition is established.

Figure 6a shows that the half bridge inverter is modelled as the fundamental component of the square waveform V_{in} and the full bridge rectifier as a resistance R_{eq1} that consumes the same average power. In Figure 6b, the leakage inductance of the receiver L_{ls} and the equivalent resistance R_{eq1} are reflected to the transmitter side, the equivalent

impedance, in parallel with the primary magnetizing inductance L_{mp}, is reduced into an equivalent inductance and resistance L_{eq1} and R_{eq2}, and finally, all the inductances are reduced in only one inductor L_{eq2} (see Figure 6c).

The first step of the analysis is to obtain the equivalent resistance of the full bridge rectifier R_{eq1}. A simplified analysis is carried out in [33], which assumes that the efficiency of the rectifier is 100%. To improve accuracy, it is possible to consider a different value for the efficiency of the rectifier (η_r) as follows:

$$\eta_r = \frac{P_o}{P_R} = \frac{P_o}{4P_D + P_o} \tag{2}$$

where P_o is the power delivered to the load (R_L) and P_R is the power delivered to the rectifier stage.

With this consideration, the equivalent resistant R_{eq1} is expressed as:

$$R_{eq_1} = \frac{8\eta_r R_L}{\pi^2} \tag{3}$$

where R_L is the load resistance.

As indicated in the introduction, the HF rectifier is one of the stages with higher losses. So, to minimize these losses, the efficiency of the rectifier is evaluated. To evaluate this efficiency, the following simplifications will be assumed:

1. The voltage at the input of the full bridge rectifier (V_o) is a square waveform in phase with the current, similar to the waveform in Figure 7, where V_o is the output voltage in the load resistance.
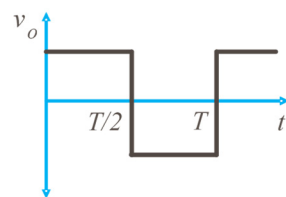

Figure 7. Assumed waveform at the input of the rectifier.

2. The input current in the rectifier is a sinusoidal waveform. Therefore, the losses in one diode can be evaluated with Equation (4).

$$P_D = I_D V_f = \frac{I V_f}{\pi} \tag{4}$$

where "I" is the maximum value of the input sinusoidal current waveform of the rectifier. This current could be expressed as $I = V_{o1}/R_{eq1}$, where V_{o1} is the fundamental of the square voltage applied to the input of the rectifier and can be expressed as:

$V_{o1} = 4V_o/\pi$. Substituting these expressions into (4):

$$P_D = \frac{V_o V_f}{2\eta_r R_L} \tag{5}$$

Substituting Equation (5) into (2), the efficiency of the rectifier could be evaluated as:

$$\eta_r = 1 - \frac{2V_f}{V_o} \tag{6}$$

This equation is plotted in Figure 8 assuming a forward voltage in the diodes $V_f = 0.7$ V. As can be seen in this figure, for an output voltage below 12 V, the efficiency abruptly decreases, so, to maintain a high efficiency, it is recommended that the output voltage verifies $V_o > 12$ V.
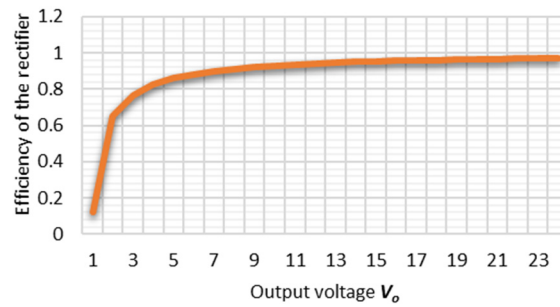
Figure 8. Efficiency of the rectifier η_r vs. the output voltage V_o (V_f = 0.7 V).

The rectifier efficiency graph in Figure 8 is presented just to show and clarify that it would work with a certain voltage level due to the efficiency of the rectifier. The graph is obtained from a simplified analysis in [33], which assumes that the efficiency of the rectifier is 100%. For this reason, the verification of this graph in the experimental tests is not necessary.

The next step is to reflect the secondary circuit of the inductive coupling to the primary circuit obtaining the circuit shown in Figure 6b. Afterwards, to obtain the equivalent impedance formed by L_{ls} and R_{eq1} (Z_{eq}), the parallel circuit of both elements is evaluated:

$$Z_{eq} = \frac{jX_{Lmp}\left(\frac{R_{eq1}+jX_{Lls}}{nt^2}\right)}{jX_{Lmp} + \frac{R_{eq1}+jX_{Lls}}{nt^2}} \tag{7}$$

Solving and simplifying Equation (7), the equivalent resistance R_{eq2} (real part of Z_{eq}) and equivalent inductance L_{eq1} (imaginary part of Z_{eq}) are obtained:

$$R_{eq2} = \frac{\frac{R_{eq1}X_{Lmp}^2}{nt^2}}{\left(\frac{R_{eq1}}{nt^2}\right)^2 + \left(X_{Lmp} + \frac{X_{L1s}}{nt^2}\right)^2} \tag{8}$$

$$L_{eq_1} = \frac{X_{Lmp}\left[\frac{X_{Lls}}{nt^2}\left(X_{Lmp} + \frac{X_{Lls}}{nt^2}\right) + \left(\frac{R_{eq1}}{nt^2}\right)^2\right]}{\omega_o\left[\left(\frac{R_{eq1}}{nt^2}\right)^2 + \left(X_{Lmp} + \frac{X_{Lls}}{nt^2}\right)^2\right]} \tag{9}$$

As can be seen in Figure 6c, the resulting equivalent circuit is a serial circuit composed of three inductances, a capacitor, and an equivalent resistance. Finally, the equivalent inductance L_{eq2} "seen" by the square input voltage V_{in} is:

$$L_{eq2} = L_c + L_{lp} + L_{eq1} \tag{10}$$

The final equivalent series circuit is shown in Figure 6c. This circuit will be in resonance when the following condition is satisfied:

$$X_{C_p} = X_{Leq2} \tag{11}$$

where X_{cp} is the reactance of C_p and X_{Leq2} is the reactance of the inductance L_{eq2}. Equation (13) can be used to calculate the necessary capacitance value C_p in order to operate the circuit at resonance. The resonance condition is important so the switching losses in the MOSFET M_1 and M_2 are as small as possible. Capacitance C_p can be calculated with the following expression:

$$C_p = \frac{1}{\omega_o^2 L_{eq2}} \tag{12}$$

Finally, to obtain the value of the compensation inductor, the following equation can be used:

$$L_c = a\left(L_{lp} + L_{eq_1}\right) \tag{13}$$

where a is a proposed value, and the higher the value of a, the lower the variation of L_{eq2}. The worst case is when the distance d is large, then $L_{lp} + L_{eq1} \approx 0$, and the relationship m between the worst case of L_{eq2} and the nominal value of L_{eq2} is:

$$m = \frac{L_{eq2w}}{L_{eq2n}} = \frac{L_c}{L_c + L_{lp} + L_{eq1}} = \frac{a}{a+1} \tag{14}$$

$$\%\text{error} = (1 - m)100 \tag{15}$$

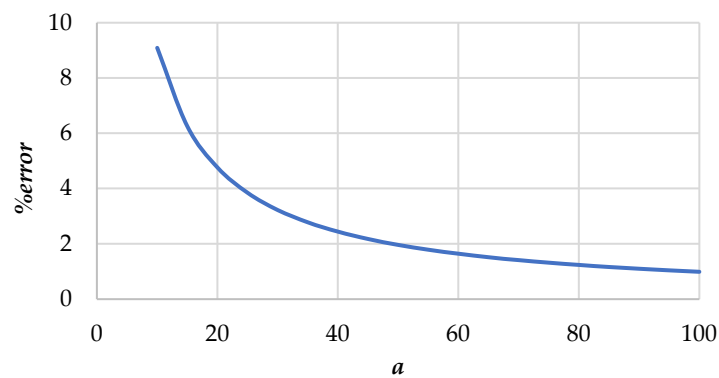Equation (16) was plotted as shown in Figure 9.

Figure 9. Percentage variations of L_{eq2} (%error) in function the factor a.

According to Figure 9, the higher the value of a, the lower the percentage of L_{eq2} variations (%error), so the compensation of the distance d variation in the transmitter and receiver misalignments will be more efficient. For example, for $a = 100$, the percentage variations of L_{eq2} (%error) are almost 1, which means no changes in L_{eq2} for large variations of d.

In this way, it is possible to compensate for the variation in the inductive coupling inductances with respect to the transmission distance and their misalignment. The circuit is expected to remain operating close to the resonance condition so that the maximum energy transfer can be achieved.

To evaluate the performance of the compensation inductor in relation to the resonance and efficiency of the circuit, three values of a will be proposed. The values will be $a = 10$, $a = 20$, and $a = 30$.

The last stage to analyze is the HF inverter, which consists of a half bridge inverter. The RMS current I_{RMS} of the resonant network (when it is operating at resonance) is obtained by applying Ohm's law using the values of the input voltage V_{in} and R_{eq2}:

$$I_{RMS} = \frac{V_{in}}{\pi R_{eq2}} \tag{16}$$

Another important characteristic to obtain is the value of average power P_M dissipated in each MOSFET of the inverter because this power represents the losses present in the inverter. In this analysis, it is recommended to select a desired dissipated power in the order of mW so that it does not affect the total efficiency of the circuit. Using the I_{RMS} and P_M values, the value of Drain-Source ON Resistance $R_{DS(on)}$ that each MOSFET should have is calculated to obtain the estimated losses in the inverter:

$$R_{DS(on)} = \frac{P_M}{I_{RMS}^2} \tag{17}$$

Substituting Equation (16) into (17):

$$R_{DS(on)} \leq \frac{P_M R_{eq_2}{}^2 \pi^2}{V_{in}{}^2} \tag{18}$$

Finally, to calculate the total efficiency η value in the proposed IPT circuit, the output power P_o (present in the load resistance) and the input power P_{in} (applied to the HF inverter) are used, which are substituted into the property of $P = VI$. Then:

$$\eta = \frac{P_o}{P_{in}}(100\%) = \frac{V_o I_o}{V_{in} I_{in}}(100\%) \tag{19}$$

3. Design Methodology

To validate the above equations, a step-by-step design methodology for the resonance condition is proposed in this work. The considered application is to charge smartphones, so the nominal distance between the transmitter and the receiver was $d = 1.5$ mm.

The design methodology to be shown is when the compensating inductor has a value of 10 times the sum of L_{lp} y L_{eq1} (a = 10). The proposed methodology is similar in cases where a = 20 or a = 30, and only the values of L_c, C_p and Q change, respectively, in each case.

Table 3 shows the design specifications, and a power of 10 W was considered for wireless chargers for smartphones and the output voltage of 12 V was selected according to Figure 8. The input voltage is considered from a small photovoltaic panel.

Table 3. Design parameters.

Parameter	Description	Value
P_o	Average output power	10 W
V_o	Output voltage	12 V
V_{in}	Input voltage	27.5 V
f_{sw}	Switching frequency	500 kHz
f_o	Resonance frequency	500 kHz
Δ_{vo}	Output voltage ripple	$5\%V_o$
a	Relationship between Lc and $(L_{lp} + L_{eq1})$	10

The design obtains the properties of the inductive coupling using the following procedure:

i.　Coupling the inductor L_p (transmitter) and L_s (receiver), correctly aligned using an acrylic plastic as the core, the thickness of the acrylic is 1.5 mm; this distance will be the transmission distance d. The inductors should not be connected to any power source or any electrical load during this measurement process.

ii.　When the inductors are coupled, an LCR tester will be used. A Hioki model 3532-50 was used in this work which is set to measure inductance at a frequency of 500 kHz; this value will be the resonance frequency at which the circuit will operate. The inductance of the primary inductor L_p (primary self-inductance) is measured by the LCR tester. Then, the inductance of the secondary inductor L_s (secondary self-inductance) is measured.

iii.　Maintaining the same conditions in the inductive coupling, the inductors L_p and L_s are connected in series, and then the measurement of the total series inductance L_T is performed with the LCR tester.

iv.　Using the values obtained in the measurements, the value of the mutual inductance M is calculated:

$$M = \frac{L_T - L_p - L_s}{2} \tag{20}$$

v.　The value of the coupling coefficient k is calculated by substituting the values of L_p, L_s and M into Equation (1).

vi.　　The primary magnetizing inductance L_{mp}, primary leakage inductance L_{lp} and secondary leakage inductance L_{ls} are calculated, and the values of these inductances are obtained using the equations presented in Table 2.

Using the method described above, the value of the inductive coupling properties shown in Table 4 can be calculated, and then the value of the IPT circuit components can be calculated using the design methodology described in Table 5.

Table 4. Characteristics of the wireless transmitter and receiver.

Parameter	Description	Value
d	Transmitter–receiver distance	1.5 mm
	Transmission medium thickness (inductive coupling core): acrylic plastic	1.5 mm
L_p	Primary self-inductance	8.625 μH
L_s	Secondary self-inductance	8.700 μH
L_T	Total series inductance	31.727 μH
L_{lp}	Primary leakage inductance. Measured short-circuiting the receiver and measuring the inductance of the primary with the nominal distance d.	1.42 μH

Table 5. Design methodology.

Parameter	Description	Equation	Value
M	Mutual inductance.	$\frac{L_T - L_p - L_s}{2}$	7.201 μH
k	Coupling coefficient.	$\frac{M}{\sqrt{L_p L_s}}$	0.831
L_{mp}	Primary Magnetizing inductance	$L_p - L_{lp}$	7.201 μH
n'	Turns relationship of the ideal transformer $n' = n'_2/n'_1$, the turns n'_1 and n'_2 represent the cross section of coils L_1 and L_2 that share the same common flux φ_M.	$\frac{M}{L_{mp}}$	1
L_{ms}	Secondary magnetizing inductance.	Mn'	7.201 μH
L_{ls}	Secondary leakage inductance.	$L_s - L_{ms}$	1.50 μH
I_o	Output current.	$\frac{P_o}{V_o}$	0.833 A
R_L	Load resistance.	$\frac{V_o^2}{P_o}$	14.4 Ω
C_f	Output filter capacitor.	$\frac{V_o}{2R_L f_o \Delta_{vR}}$	3.49 μF
n_{Rect}	Full bridge rectifier efficiency.	$1 - \frac{2V_f}{V_o}$	0.89
I_D	Diode average current	$\frac{I_o}{2}$	0.417 A
L_c	Compensation inductor.	$a\left(L_{lp} + L_{eq_1}\right)$	34.31 μH
C_p	Primary capacitor.	$\frac{1}{(2\pi f_o)^2 (1.1 L_c)}$	2.711 nF
Q	Quality factor	$\frac{X_{C_p}}{R_{eq_2}}$	18.88
$R_{DS(on)}$	Drain-Source ON Resistance	$\leq \frac{P_M R_{eq_2}^2 \pi^2}{V_{in}^2}$	≤20 mΩ
η	Total efficiency of the IPT circuit	$\frac{P_o}{P_{in}}(100\%)$	75%

Table 4 presents the characteristics of the wireless transmitter and receiver, the IPT inductors were model WE760308111 from Würth Electronics.

Table 5 presents the design methodology, where the nominal distance d = 1.5 mm, which is the thickness of the acrylic between the transmitter and the receiver.

For the implementation of the full bridge rectifier located in the receiver circuit, the MUR840 diodes were selected. This diode model supports an average current of 8A.

The MOSFET IRFZ46N was selected for the high-frequency inverter located in the transmitter circuit. This MOSFET model has an $R_{DS(on)}$ of 16.5 mΩ

3.1. Implementation of Compensation Inductor Lc

The compensation inductor used for the TPI circuit was manufactured with Litz wire, which is composed of a wire number N_w of 160 wires and each copper wire is 44 AWG. The length of the conductor l_c is 3.56 m. The compensation inductor is made up of 63 turns, using an ETD29 model that is shown in Figure 10.
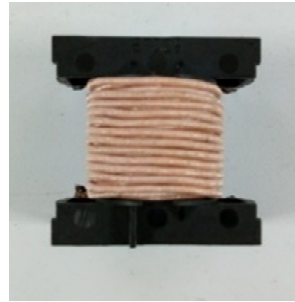

Figure 10. Picture of the compensation inductor L_C picture used in the IPT circuit.

The compensation inductor designed for the TPI circuit has an air core, so the only losses that occur in the component are conduction losses in the copper of the inductor. The copper presents a parasitic resistance that will oppose the flow of electric current through the inductor. Equation (21) presents the formula to obtain the parasitic resistance of the inductor R_{Lc}.

$$R_{Lc} = \frac{\rho_{cu} l_c}{N_w A_c} \tag{21}$$

where ρ_{cu} is the copper resistivity (17.2×10^{-9} Ω·m), l_c is the length of the conductor (3.56 m), N_w is the wire number (160 wires) and A_c is the wire cross sectional area (2.463×10^{-9} m^2). Substituting these values into Equation (21):

$$R_{Lc} = \frac{(17.2 \times 10^{-9} \ \Omega \cdot \text{m})(3.56 \ \text{m})}{(160)(2.463 \times 10^{-9} \ \text{m}^2)} = 155.37 \ \text{m}\Omega \tag{22}$$

3.2. Determination of the Properties of the Inductive Coupling with Different Distances d

In the design methodology, the value of the IPT circuit components was obtained to work correctly at distance d = 1.5 mm. As the circuit is oriented to wireless charging applications of smartphones, it is important to consider that during wireless charging there may be changes in the transmission distance with different causes; these changes directly affect the properties of the inductive coupling, modifying their value.

For that reason, before starting with the implementation of the designed circuit, the measurement and calculation of the inductive coupling properties at different distances d must be performed using the procedure shown at the beginning of Section 3. In the procedure, it is established that the transmission inductors during the measurements should not be connected to any power supply or any electrical load; for this reason, the measurements of the inductive coupling should be performed before the assembly of the IPT circuit on the PCB.

Ten transmission distances were selected as test points to perform measurements of the inductive coupling, with the objective of watching the changes in the coupling with respect to the distance d. This circuit being of the near-field WTP type, the inductor L_s will be moving away from L_p and the plastic acrylic (coupling core) from a distance of 1.5 mm to 4 mm; therefore, there will be 11 measured values for each property of the inductive coupling. The measured and calculated values at each transmission distance are L_p, L_s, L_T, M and k.

The LCR tester was used to measure the inductances, while a digital Vernier was used for the transmission distances d. The measured and calculated results are presented in Table 6.

Table 6. Obtained values of inductive coupling properties at different transmission distances *d*.

d (mm)	L_p (µH)	L_s (µH)	L_T (µH)	*M* (µH)	*k*
1.5	8.625	8.700	31.727	7.201	0.831
1.8	8.558	8.624	31.288	7.053	0.821
2	8.392	8.467	30.547	6.844	0.812
2.2	8.268	8.343	29.931	6.660	0.802
2.5	8.146	8.208	29.306	6.476	0.792
2.8	8.053	8.097	28.794	6.322	0.783
3	7.934	7.989	28.233	6.155	0.773
3.2	7.819	7.864	27.649	5.983	0.763
3.5	7.708	7.746	27.090	5.818	0.753
3.8	7.582	7.623	26.517	5.656	0.744
4	7.496	7.531	26.055	5.514	0.734

4. Experimental Results

A prototype was implemented to experimentally test the circuit in Figure 5 to validate the design methodology shown in Table 5. Figures 11 and 12 show the implementation of the inductive IPT circuit.
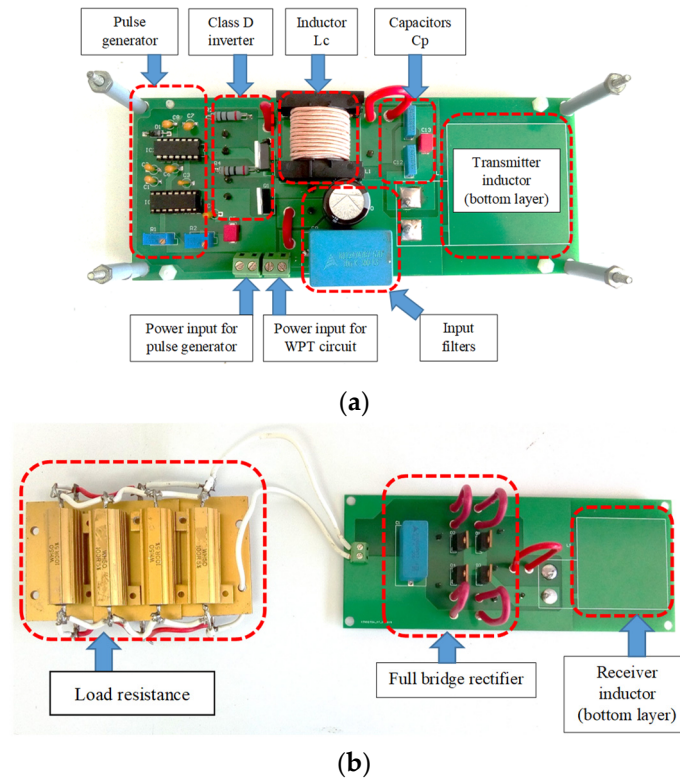

(**a**)

(**b**)

Figure 11. Implementation of the inductive IPT circuit, (**a**) transmitter device, (**b**) receiver device.
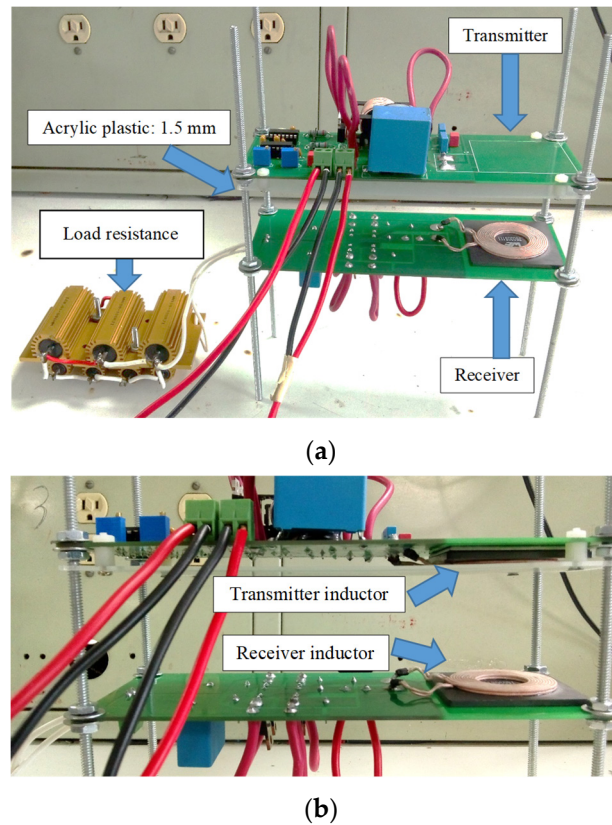
(**a**)

(**b**)

Figure 12. Prototype experimental assembly, (**a**) prototype test bench, (**b**) view of transmission distance setting (adjustable range from 1.5 mm to 4 mm).

To validate the design conditions, the prototype was adjusted with an initial transmission distance of 1.5 mm. Experimental results are shown in Figure 13. Figure 13a shows the output voltage, output current, and output power. Figure 13b shows the input voltage, input current and input power. The measured values are shown in Table 7, which comply with the design parameters established in Table 3.

Table 7. Experimental results obtained at nominal conditions.

Parameter	Description	Measured Value
P_o	Output power	10.59 W
V_o	Output voltage	12 V
I_o	Output current	0.881 A
V_{in}	Input voltage	27.5 V
I_{in}	Input current	0.5129 A
P_{in}	Input power	14.1 W
η	Total circuit efficiency	75.10%
f_o	Resonance frequency	497.4 kHz
ϕ	Phase offset angle	0.1074°

The input voltage was adjusted to deliver the nominal voltage to the load. Figure 13c shows the square voltage applied to the resonant tank and the current in the compensation inductor. As can be seen in this figure, the current is in phase with the voltage; therefore, the circuit is in resonance. These results validate the proposed design methodology since they are very similar to the theoretical ones.
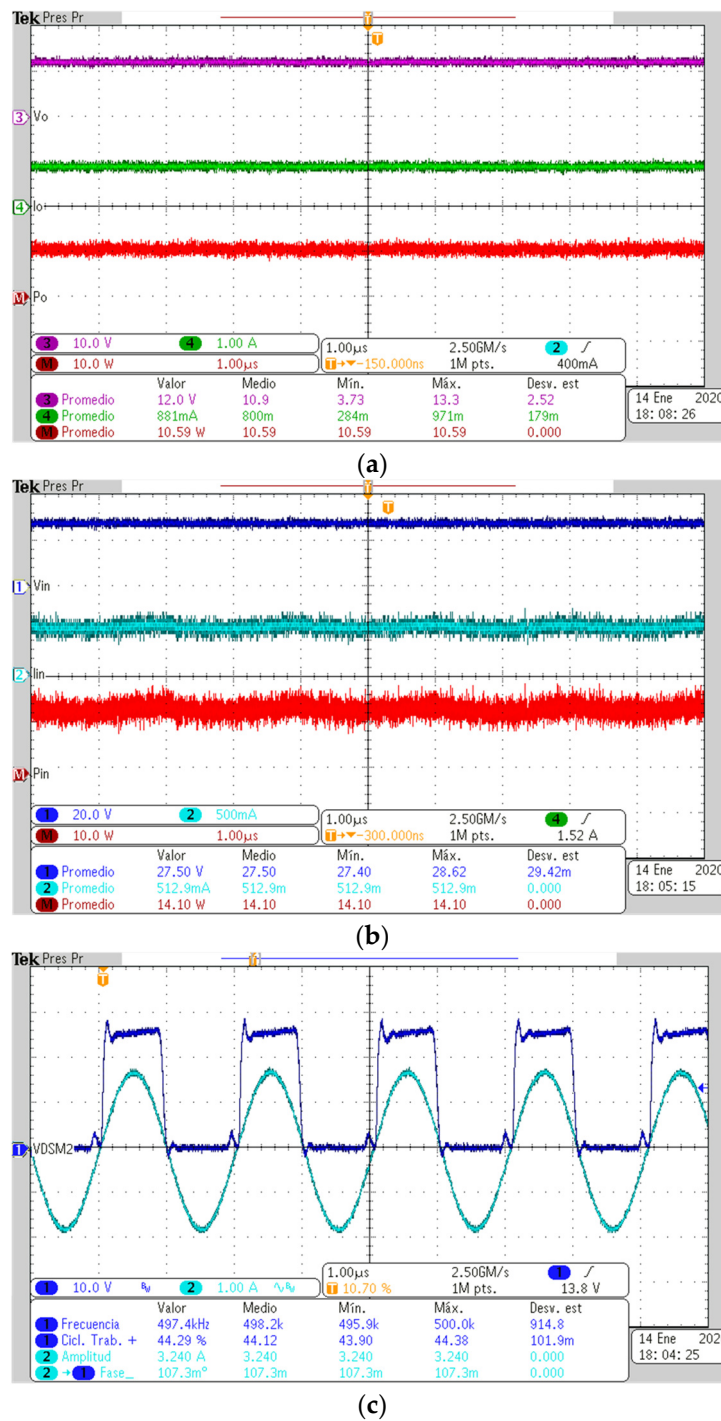
(**a**)

(**b**)

(**c**)

Figure 13. (**a**) Channel 3: output voltage V_o, 10 V/div (purple). Channel 4: output current I_o, 1 A/div (green). Math Channel: output power P_o, 10 W/div (red). (**b**) Channel 1: input voltage, 20 V/div (navy blue). Channel 2: input current, 500 mA/div (light blue). Math Channel: input power, 10 W/div (red). (**c**) Channel 1: class D inverter output voltage, 10 V/div (navy blue). Channel 2: resonant network current, 1 A/div (light blue).

The total efficiency η of the IPT circuit is calculated using Equation (19) and the values obtained in the measurements of P_{in} and P_o, which are presented in Figure 13a,b.

$$\eta = \frac{10.59\,\text{W}}{14.10\,\text{W}}(100\%) = 75.10\% \tag{23}$$

Experimental Results with Different Distances "d"

To test the robustness of the circuit for changes in the transmission distance. Ten different test points were performed from 1.5 mm to 4 mm. The following variables were measured: output voltage (V_o), output power (P_o), input power (P_{in}), total efficiency (η) and phase offset (ϕ). The experimental results obtained were compared with the k values obtained in Section 3.2, and the values together are shown in Table 8.

Table 8. Experimental results obtained by modifying the transmission distance from 1.5 mm to 4 mm (a = 10).

d (mm)	k	V_o (V)	P_o (W)	P_{in} (W)	η (%)	ϕ (°)
1.5	0.831	12.00	10.59	14.10	75.10	0.10
1.8	0.821	11.71	10.07	13.51	74.55	−7.74
2	0.812	11.70	10.05	13.60	73.93	−14.40
2.2	0.802	11.36	9.46	12.84	73.70	−16.74
2.5	0.792	11.11	9.07	12.35	73.41	−17.50
2.8	0.783	10.83	8.61	11.85	72.65	−18.68
3	0.773	10.57	8.21	11.58	70.84	−19.44
3.2	0.763	10.34	7.85	11.61	67.61	−21.61
3.5	0.753	10.14	7.54	11.84	63.72	−22.15
3.8	0.744	9.97	7.30	12.31	59.31	−37.46
4	0.734	8.56	5.62	10.37	54.29	−39.18

Using the same design methodology already shown, the value of the compensation inductor L_c is calculated. The value of L_c is obtained using Equation (14) when it is 20 (a = 20) and 30 (a = 30) times the sum of L_{lp} y L_{eq1}. The calculation of L_c and C_p when a = 20 is shown in Table 9, while the a = 30 calculation is shown in Table 10.

Table 9. Calculation of L_c and C_p when a = 20.

Parameter	Description	Equation	Value
L_c	Compensation inductor.	$a\left(L_{lp} + L_{eq_1}\right)$	68.62 µH
C_p	Primary capacitor.	$\dfrac{1}{(2\pi f_o)^2(1.03L_c)}$	1.406 nF

Table 10. Calculation of L_c and C_p when a = 30.

Parameter	Description	Equation	Value
L_c	Compensation inductor.	$a\left(L_{lp} + L_{eq_1}\right)$	102.93 µH
C_p	Primary capacitor.	$\dfrac{1}{(2\pi f_o)^2(1.03L_c)}$	0.952 nF

These new values of L_c and C_p were implemented in the IPT circuit for each case, and experimental tests were performed at different transmission distances using the same method as the tests shown in Table 8. The results are shown in Tables 11 and 12.

Analyzing the results obtained in Table 7, we can see that the coupling coefficient has a value of 0.734 for a transmission distance of 4 mm. This table shows the output voltage, which falls to 8.56 V when the transmission distance is 4 mm—more than double the nominal value. The output power in this table falls to 5.62 W for a transmission distance of 4 mm. The input power decreases with the transmission distance until a transmission distance of 4 mm. For d = 4 mm, the phase offset angle (ϕ) increases from zero to 39°. The efficiency falls to 54.29% for d = 4 mm.

Comparing the results obtained in Table 8 with the results of Tables 11 and 12, it can be observed that the coupling coefficient, the output voltage, the output power, and the phase angle present the same behaviour, slightly changing their values when the transmission distance increases up to 4 mm.

Table 11. Experimental results obtained when ($a = 20$).

d (mm)	k	V_o (V)	P_o (W)	P_{in} (W)	η (%)	ϕ (°)
1.5	0.831	12.00	10.57	14.49	72.95	0.15
1.8	0.821	11.86	10.33	15.26	67.67	−3.24
2	0.812	11.75	10.14	15.21	66.65	−7.02
2.2	0.802	11.54	9.78	15.14	64.59	−10.44
2.5	0.792	11.38	9.51	15.08	63.04	−11.98
2.8	0.783	11.16	9.14	14.95	61.16	−12.96
3	0.773	11.11	9.06	14.93	60.70	−14.40
3.2	0.763	10.86	8.66	14.88	58.19	−15.30
3.5	0.753	10.34	7.85	14.05	55.89	−18.00
3.8	0.744	9.70	6.91	13.44	51.43	−18.36
4	0.734	9.09	6.07	12.22	49.68	−21.78

Table 12. Experimental results obtained when ($a = 30$).

d (mm)	k	V_o (V)	P_o (W)	P_{in} (W)	η (%)	ϕ (°)
1.5	0.831	12.00	10.68	15.18	70.40	0.13
1.8	0.821	11.98	10.64	15.71	67.74	−1.31
2	0.812	11.95	10.60	16.13	65.74	−3.29
2.2	0.802	11.93	10.55	16.16	65.28	−8.87
2.5	0.792	11.86	10.54	16.75	62.90	−9.05
2.8	0.783	11.84	10.39	17.23	60.30	−10.25
3	0.773	11.72	10.38	17.36	59.81	−10.89
3.2	0.763	11.57	10.27	17.44	58.87	−11.58
3.5	0.753	11.38	10.17	17.41	58.41	−12.53
3.8	0.744	11.19	10.09	17.28	58.40	−13.42
4	0.734	10.97	9.90	17.03	58.15	−15.35

The results obtained in the tables show the following:

- The output voltage value decreases to 10.97 V, although it stays closer to 12 V, as the value of a increases.
- The output power value decreases to 9.9 W, staying closer to 10 W, as the value of a increases.
- The total efficiency at a transmission distance of 1.5 mm decreases minimally as the value of a increases. This is because the value of a increases and the value of the inductor wire resistance increases with it.
- The 10-phase angle (ϕ) stays closer to resonance as the value of a increases. As the inductor value a increases, it will better compensate for the variations caused by misalignment and transmission distance.

From these results, it is observed that the compensation inductor can compensate for changes at the transmission distance of twice the nominal distance of 1.5 mm, achieving a total efficiency of 75.10%. It is important to clarify that the prototype was designed to operate over a wide range of powers and distances between the transmitter and receiver. A specific design for a fixed distance "d", optimizing the design of the inductor L_c as well as the selection of the semiconductors, and changing them for SiC or GaN semiconductors, can substantially increase the efficiency.

There is a tradeoff between the size of the inductor L_c and the distance "d"; the greater the distance "d", the larger the inductor L_c required. However, with a higher switching frequency, an excessively large inductor L_c will not be required.

The main disadvantage of the proposal is that the proposed solution is passive. To compensate better for the misalignment and greater distances between the transmitter and receiver, it is recommended to combine this proposal with others such as closed-loop operation and solutions for better coupling factors.

5. Conclusions

This work introduced a very simple compensation topology that consists of only one inductor useful for resonant IPT circuits operating in an open loop for low-power applications and small transmission distance applications (near-field applications), such as wireless chargers of cell phones. To compensate for changes in the transmission distance and misalignment of the transmitter and receiver, only one compensation inductor is added to the resonant tank.

A sufficiently bigger inductor is chosen to maintain the resonant tank operating near resonance for changes until the nominal transmission distance is doubled. The analysis and design methodology for the inductive coupling was presented to establish the resonance condition. The experimental results validate the proposed design methodology. In addition, they confirm the correct functioning of the circuit.

The experimental results obtained under the design conditions validate the proposed design methodology with a maximum error of 5.9% in the output power. A total efficiency of 75% was achieved at a fixed transmission distance of 1.5 mm, using acrylic as a transmission medium.

The implemented circuit operates very near to the resonance condition; comparing the theoretical design values with the experimental results, errors of 0.059% in the phase shift angle and 0.02% in the resonance frequency are obtained.

The results obtained by modifying the transmission distance demonstrate the presence of inductance variations in the inductive coupling as the transmitter inductor moves away from the receiver inductor. However, these variations could be compensated for with only one inductor used instead of more complex compensation topologies. For small variations of the transmission distances (twice or three times), this inductor compensated for the variations in the mutual inductance and self-inductances of the transmitter due to the changes in the coupling factor.

According to the obtained results, the proposed circuit is a good option as a wireless charger for cell phones in which the application transmits power over very short distances.

The circuit proposed in this work is limited to applications where the transmission distance is larger because these applications are of the far-field WPT type. In this type of application, where the distance is large, it would affect the design of the circuit presented in several ways, such as the following:

- The size of the inductors L_p and L_s would increase considerably in order to realize the wireless power transmission through inductive coupling.
- The input voltage V_{in} would need to be increased considerably to compensate for the losses in the inductive coupling, because over long distances, the inductive coupling coefficient k is usually small and the power transmission efficiency from L_p to L_s is low.
- The size and the value of the compensation inductor L_c would increase because it must compensate for the misalignment of the inductors L_p and L_s in addition to trying to keep the circuit in resonance at a larger transmission distance. As the size of the inductor L_c increases, the series parasitic resistance R_{Lc} in the inductor also increases due to the length of the copper conductor, presenting a higher amount of losses in the IPT circuit.
- As the value of the inductor L_c increases, as a consequence, the value of the primary capacitor C_p will decrease considerably, achieving a value that is difficult to implement because it will be valued in the order of pF or less.
- The total efficiency will be low due to the losses present in the inductive coupling. In this type of application, it is recommended to combine the circuit proposed in this work with a closed-loop method that allows to adjust the resonance and bring the maximum power transfer from L_p to L_s.

The IPT circuit proposed in this work was validated and works adequately inside the limits previously described; therefore, it is recommended to be used in near-field WPT-type applications and for low-power electronic devices.

6. Discussion

This section will present an in-depth analysis of the results obtained, some of which were not mentioned in the previous sections, as well as some general characteristics, recommendations, contributions of this work, and possible future works to give continuity to the presented topic.

6.1. Relevant Conclusions

Once the work developed in this paper is completed, the following conclusions can be drawn:

- The resonant network suitable for low-power inductive IPT applications is the series-series topology with inductive coupling; due to this resonant network, operating in resonance has a unity voltage gain. For this reason, the series–series topology was selected for the IPT circuit designed.
- An analysis and design methodology was developed for the proposed resonant network, which will allow the proposed IPT circuit to operate according to the desired design specifications.
- The experimental results obtained validate the analysis and design methodology proposed in this work.
- The implemented IPT circuit enables wireless power transmission from a DC voltage source to an electrical load using resonant inductive coupling to perform the transmission.

6.2. General Characteristics of the Implemented IPT Circuit

The IPT circuit implemented in this work has the following characteristics:

- The implemented IPT circuit works according to the desired design specifications: 12 volts at the output, 10 watts at the output, the resonant network is in resonance, and the circuit performs the wireless power transmission.
- The IPT circuit achieves a total efficiency of 75.10% under the design conditions (stationary distance, transmission medium: plastic acrylic of 1.5 mm thickness).
- It is an easy-to-implement circuit because it operates in an open loop.
- The prototype is suitable for inductive wireless charging applications, as long as low-power applications are no greater than 10 W.
- The IPT circuit allows a horizon of wireless battery-charging applications, such as cell phones, electric toothbrushes, electric shavers, portable hearing aids, and hand lamps, among others.
- The transmitting inductors do not present a temperature rise because they only provide 10% of the inductive reactance of the resonant network.

6.3. Recommendations

To achieve a successful implementation of the proposed IPT circuit, it is recommended to consider the following:

- It is important to consider that this circuit is for near-field WPT-type applications, especially for wireless charging of low-power wireless devices.
- For the selection of the diodes of the full bridge rectifier in the secondary circuit, it is recommended to use ultra-fast diodes that are capable of operating correctly at high switching frequencies.
- For the implementation of the compensation inductor Lc, it is recommended to use Litz wire because it will reduce the series parasitic resistance R_{Lc} of this inductor.
- The transmission inductors L_p and L_s must be identical in structure, inductance, design and size to achieve an efficient coupling coefficient k. It is recommended to use two inductors of the same model designed for IPT applications.
- For the selection of the MOSFETs of the high-frequency inverter, it is recommended to use a device with the lowest possible $R_{DS(on)}$ to avoid the highest possible conduction losses in the device.

6.4. Contributions of This Work

The work developed has the following contributions:

- An analysis methodology is contributed for the resonant network of an inductive IPT circuit, in which all the inductances of the inductive coupling are considered as part of a single resonant tank. The literature uses two independent resonant tanks for the analysis—one in the transmitter circuit and one in the receiver circuit.
- A resonant network topology used for inductive IPT is presented, where a single capacitor is used, which is different from the literature, where two are used (one in the transmitter and one in the receiver); in addition, a compensation inductor is used that contributes 90% of the inductive reactance in the resonant condition [34].
- A prototype for inductive IPT that is capable of performing wireless power transmission is provided. Such a device is useful in wireless battery-charging applications for low power.

6.5. Possible Future Work

Considering the importance of the resonance and coupling coefficient of the IPT circuit together with the experience obtained in this work, the following recommendations are presented for possible future work:

- To apply a PLL control loop that allows maintaining the resonance of the resonant network under variations in the inductive coupling. Such variations can be caused by the temperature, the misalignment of the transmission inductors or the transmission distance between both inductors.
- To use a control technique with active diodes in the rectification stage, which is located in the receiver device, in order to improve the efficiency of the rectifier and consequently the total efficiency of the IPT circuit.
- Investigate and apply techniques that improve the inductive coupling coefficient in order to improve the efficiency of wireless power transmission. The techniques can be related to the geometry of the transmitting inductors and the use of multiple transmitting inductors.
- In order to improve the inductive coupling coefficient, the resonant network can be used as an analogue frequency multiplier. The resonant network receives at the input the switching frequency of the inverter, and then a sinusoidal signal with a frequency multiplied "n" times the switching frequency can be delivered to the output. The signal delivered at the output will be the resonant frequency of the resonant network. This method is presented in [4].

These proposals are suggested to give continuity to this work.

Conflicts of Interest: The authors declare no conflict of interest.

References

1. Tran, M.T.; Thekkan, S.; Polat, H.; Tran, D.-D.; El Baghdadi, M.; Hegazy, O. Inductive Wireless Power Transfer Systems for Low-Voltage and High-Current Electric Mobility Applications: Review and Design Example. *Energies* **2023**, *16*, 2953. [CrossRef]
2. Laha, A.; Kalathy, A.; Pahlevani, M.; Jain, P. A Comprehensive Review on Wireless Power Transfer Systems for Charging Portable Electronics. *Eng* **2023**, *4*, 1023–1057. [CrossRef]

3. Zhang, Z.; Pang, H. *The Era of Wireless Power Transfer*; John Wiley & Sons, Inc.: Hoboken, NJ, USA, 2023.

4. Lara-Reyes, J.; Ponce-Silva, M.; Hernández-González, L.; DeLeón-Aldaco, S.E.; Cortés-García, C.; Ramirez-Hernandez, J. Series RLC Resonant Circuit Used as Frequency Multiplier. *Energies* **2022**, *15*, 9334. [CrossRef]

5. Manivannan, B.; Kathirvelu, P.; Balasubramanian, R. A review on wireless charging methods—The prospects for future charging of EV. *Renew. Energy Focus* **2023**, *46*, 68–87. [CrossRef]

6. Yoo, J.-S.; Gil, Y.-M.; Ahn, T.-Y. High-Power-Density DC–DC Converter Using a Fixed-Type Wireless Power Transmission Transformer with Ceramic Insulation Layer. *Energies* **2022**, *15*, 9006. [CrossRef]

7. Ibrahim, H.H.; Singh, M.J.; Al-Bawri, S.S.; Ibrahim, S.K.; Islam, M.T.; Alzamil, A.; Islam, M.S. Radio frequency energy harvesting technologies: A comprehensive review on designing, methodologies, and potential applications. *Sensors* **2022**, *22*, 4144. [CrossRef]

8. Mahesh, M.; Kumar, K.V.; Abebe, M.; Udayakumar, L.; Mathankumar, M. A review on enabling technologies for high power density power electronic applications. *Mater. Today Proc.* **2021**, *46*, 3888–3892. [CrossRef]

9. Shakil, S.; Rashid, M.H. The potential impacts of wireless power transfer on the global economy, society, and environment. In Proceedings of the IEEE 14th Power Electronics, Drive Systems, and Technologies Conference (PEDSTC), Babol, Iran, 31 January–2 February 2023; pp. 1–5.

10. Iam, I.-W.; Choi, C.-K.; Lam, C.-S.; Mak, P.-I.; Martins, R.P. A constant-power and optimal-transfer-efficiency wireless inductive power transfer converter for battery charger. *IEEE Trans. Ind. Electron.* **2023**, *71*, 450–461. [CrossRef]

11. Okasili, I.; Elkhateb, A.; Littler, T. A Review of Wireless Power Transfer Systems for Electric Vehicle Battery Charging with a Focus on Inductive Coupling. *Electronics* **2022**, *11*, 1355. [CrossRef]

12. Wu, M.; Su, L.; Chen, J.; Duan, X.; Wu, D.; Cheng, Y.; Jiang, Y. Development and Prospect of Wireless Power Transfer Technology Used to Power Unmanned Aerial Vehicle. *Electronics* **2022**, *11*, 2297. [CrossRef]

13. Lara-Reyes, J.; Ponce-Silva, M.; Cortés-García, C.; Lozoya-Ponce, R.E.; Parrilla-Rubio, S.M.; García-García, A.R. High-Power-Factor LC Series Resonant Converter Operating Off-Resonance with Inductors Elaborated with a Composed Material of Resin/Iron Powder. *Electronics* **2022**, *11*, 3761. [CrossRef]

14. Benalia, N.; Laroussi, K.; Benlaloui, I. Improvement of the Magnetic Coupler design for Wireless Inductive Power Transfer. In Proceedings of the IEEE 5th International Conference on Power Electronics and their Applications (ICPEA), Hail, Saudi Arabia, 29–31 March 2022; Volume 1, pp. 1–6.

15. Oshimoto, N.; Sakuma, K.; Sekiya, N. Improvement in Power Transmission Efficiency of Wireless Power Transfer System Using Superconducting Intermediate Coil. *IEEE Trans. Appl. Supercond.* **2023**, *33*, 1501004. [CrossRef]

16. Rayan, B.A.; Subramaniam, U.; Balamurugan, S. Wireless Power Transfer in Electric Vehicles: A Review on Compensation Topologies, Coil Structures, and Safety Aspects. *Energies* **2023**, *16*, 3084. [CrossRef]

17. Chowdhury, S.A.; Kim, S.; Kim, S.; Moon, J.; Cho, I.; Ahn, D. Automatic Tuning Resonant Capacitor to Fix the Bidirectional Detuning with ZVS in Wireless Power Transfer. *IEEE Trans. Ind. Electron.* **2023**, 1–10. [CrossRef]

18. Brovont, A.D.; Aliprantis, D.; Pekarek, S.D.; Vickers, C.J.; Mehar, V. Magnetic Design for Three-Phase Dynamic Wireless Power Transfer with Constant Output Power. *IEEE Trans. Energy Convers.* **2023**, *38*, 1481–1484. [CrossRef]

19. Zhou, Y.; Qiu, M.; Wang, Q.; Ma, Z.; Sun, H.; Zhang, X. Research on Double LCC Compensation Network for Multi-Resonant Point Switching in Underwater Wireless Power Transfer System. *Electronics* **2023**, *12*, 2798. [CrossRef]

20. Yoo, J.-S.; Gil, Y.-M.; Ahn, T.-Y. Steady-State Analysis and Optimal Design of an LLC Resonant Converter Considering Internal Loss Resistance. *Energies* **2022**, *15*, 8144. [CrossRef]

21. Li, Q.; Duan, S.; Fu, H. Analysis and Design of Single-Ended Resonant Converter for Wireless Power Transfer Systems. *Sensors* **2022**, *22*, 5617. [CrossRef]

22. Kamali, R.; Gholamian, S.A.; Abdollahi, S.R. An Investigation on Selecting of Resonant Inverter Topologies for Efficient Wireless Power Transmission. In Proceedings of the IEEE 14th Power Electronics, Drive Systems, and Technologies Conference (PEDSTC), Babol, Iran, 31 January–2 February 2023; pp. 1–6.

23. Feng, H.; Cai, T.; Duan, S.; Zhao, J.; Zhang, X.; Chen, C. An LCC-Compensated Resonant Converter Optimized for Robust Reaction to Large Coupling Variation in Dynamic Wireless Power Transfer. *IEEE Trans. Ind. Electron.* **2016**, *63*, 6591–6601. [CrossRef]

24. Dai, X.; Qiu, N. Insensitive design for wireless power transfer system using LLC resonant converter. In Proceedings of the 2016 Progress in Electromagnetic Research Symposium (PIERS), Shanghai, China, 8–11 August 2016; pp. 5193–5198.

25. Jang, Y.; Han, J.-K.; Baek, J.-I.; Moon, G.-W.; Kim, J.-M.; Sohn, H. Novel multi-coil resonator design for wireless power transfer through reinforced concrete structure with rebar array. In Proceedings of the IEEE 3rd International Future Energy Electronics Conference and ECCE Asia (IFEEC 2017-ECCE Asia), Kaohsiung, Taiwan, 3–7 June 2017; pp. 2238–2243.

26. Sun, K.; Wang, J.; Burgos, R.; Boroyevich, D. A series-series-CL resonant converter for wireless power transfer in auxiliary power network. In Proceedings of the IEEE Applied Power Electronics Conference and Exposition (APEC), New Orleans, LA, USA, 15–19 March 2020; pp. 813–818.

27. Aldhaher, S.; Luk, P.C.-K.; Whidborne, J.F. Tuning Class E Inverters Applied in Inductive Links Using Saturable Reactors. *IEEE Trans. Power Electron.* **2013**, *29*, 2969–2978. [CrossRef]

28. Iannuzzi, D.; Rubino, L.; Di Noia, L.P.; Rubino, G.; Marino, P. Resonant inductive power transfer for an E-bike charging station. *Electr. Power Syst. Res.* **2016**, *140*, 631–642. [CrossRef]

29. Shi, L.; Alou, P.; Oliver, J.A.; Cobos, J.A. A Novel Self-adaptive Wireless Power Transfer System to Cancel the Reactance of the Series Resonant Tank and Deliver More Power. In Proceedings of the IEEE Energy Conversion Congress and Exposition, Baltimore, MD, USA, 29 September–3 October 2019; pp. 4207–4211.

30. Berger, A.; Agostinelli, M.; Vesti, S.; Oliver, J.A.; Cobos, J.A.; Huemer, M. A Wireless Charging System Applying Phase-Shift and Amplitude Control to Maximize Efficiency and Extractable Power. *IEEE Trans. Power Electron.* **2015**, *30*, 6338–6348. [CrossRef]

31. Ondin, U.; Balikci, A. A Transformer Design for High-Voltage Application Using LLC Resonant Converter. *Energies* **2023**, *16*, 1377. [CrossRef]

32. Yao, W.; Lu, J.; Taghizadeh, F.; Bai, F.; Seagar, A. Integration of SiC Devices and High-Frequency Transformer for High-Power Renewable Energy Applications. *Energies* **2023**, *16*, 1538. [CrossRef]

33. Erickson, R.W.; Maksimovic, D. *Fundamentals of Power Electronics*; Springer Science & Business Media: Berlin/Heidelberg, Germany, 2007; pp. 712–713.

34. García-García, A.R.; Ponce-Silva, M.; Cortés-García, C. Dispositivo para Transmisión de Potencia Inalámbrica—Device for Wireless Power Transmission. Mexico, Patent Application: MX/a/2020/011304, Mexican Institute of Industrial Property. 2020. Available online: https://vidoc.impi.gob.mx/visor?usr=SIGA&texp=SI&tdoc=E&id=MX/a/2020/011304 (accessed on 2 July 2023).